Decoherence in large NMR quantum registers

Hans Georg Krojanski and Dieter Suter
Universität Dortmund, Fachbereich Physik, 44221 Dortmund, Germany
(Received 22 September 2006; published 26 December 2006)

Decoherence causes the decay of the quantum information that is stored in highly correlated states during quantum computation. It is thus a limiting factor for all implementations of a quantum computer. Because a scalable quantum computer with hundreds or thousands of qubits is not available yet, experimental data about decoherence rates was restricted to small quantum registers. With solid state nuclear magnetic resonance we create highly correlated multiqubit states that serve as a model quantum register and measure their decay. By measuring the decay as a function of the system size, we determined the scaling of the decoherence rate with the number of qubits. Using the same system, we also used decoupling techniques to reduce the coupling between system and environment and thereby the decoherence rate by more than an order of magnitude, independent of the system size. For the free decay as well as for the decoupled case, we found a relatively weak scaling with system size, which could be fitted to a power law $\propto \bar{K}^p$ with an exponent $p \approx 1/2$. This raises the prospect for large-scale quantum computation.

DOI: 10.1103/PhysRevA.74.062319 PACS number(s): 03.67.−a, 03.65.Yz

I. INTRODUCTION

Quantum computers are capable of efficiently solving computational problems that cannot be solved efficiently by classical computers. The most popular example may be Shor's algorithm for the decomposition of (large) numbers into their prime factors [1]. For the best-known classical algorithm for this problem, the number field sieve, the execution time grows (sub)exponentially with the number of digits n of the input [2]. In contrast to this, the execution time for Shor's algorithm grows only as a polynomial function of n.

Useful implementations of such quantum algorithms will have to operate on large quantum registers consisting of thousands of qubits to tackle problems that cannot be solved by classical computers. The main difficulty for the implementation of such large-scale quantum information processing is to make it robust, i.e., to minimize the number of errors that occur either due to imperfect gate operations or due to unwanted interactions with the environment.

The loss of quantum information due to uncontrollable interactions of the qubits with their environment is called decoherence. This will probably be the largest obstacle to an increased quantum register size, because it is expected that decoherence is faster in larger systems. Several schemes have been proposed for scalable implementations of quantum information processing on the basis of superconductors [3], semiconductors [4], ion traps [5], or spins in solids [6–12]. In all such systems, decoherence times were measured or estimated only for individual qubits.

To be able to extrapolate decoherence rates to larger (and thus more powerful) quantum registers, we measured decoherence rates in model quantum registers consisting of highly correlated spin states as a function of the number of qubits and found a relatively benign scaling behavior [13].

If the failure probability in individual quantum gates is below a certain threshold, then it is possible to perform reliably arbitrarily long quantum computations by using quantum error correction [14,15]. To reach this threshold, or if the decoherence processes are too fast for a direct application of quantum error correction, it is proposed to reduce the decoherence processes by introducing an additional time dependence on the quantum system [16,17] that averages the interaction with the environment to zero (or a smaller value). Such schemes are well known in small systems [18–24], and recently we were able to show that they also can be applied to large quantum registers [25].

In this paper, we discuss in detail the scaling behavior of the decoherence rate in model quantum registers with several 1000 qubits, consisting of nuclear spins in a simple solid. While these qubits are not individually addressable and therefore not suitable for implementing quantum algorithms, they are ideally suited for the study of decoherence processes. In particular, they allow not only the measurement of the decoherence rate of the spins, but we could also apply (global) gate operations that implement a suitable decoupling algorithm. For this decoupling procedure, we experimentally determined the efficiency (i.e., the reduction of the decoherence rate) and the scaling behavior with the number of qubits.

The paper is organized as follows: In Sec. II we explain the principle of the experiment and discuss the relevant Hilbert space and the creation of the model quantum register. The measurement of the quantum register size and accompanying experimental results are presented in Sec. III. The principle of the decoherence measurements is elucidated in Sec. IV, where we also show the scaling of the decoherence rates for full coupling between the qubits and their environment. These results are compared in Sec. V with the decoherence rates obtained under decoupling. The concluding section summarizes the results.

II. QUANTUM REGISTER

A. Experimental principle

To measure the decoherence rate in large quantum registers, we first have to prepare a state that includes quantum correlations between a large number of qubits (nuclear spins

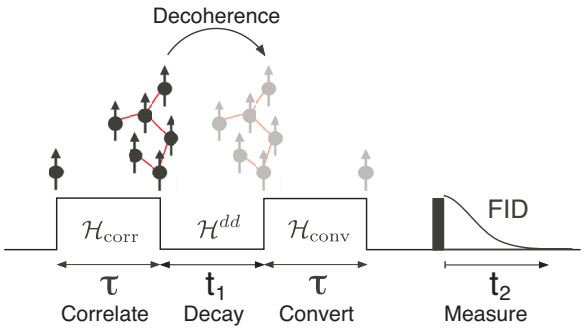

FIG. 1. (Color online) Experimental scheme: The (effective) Hamiltonian $\mathcal{H}_{\rm corr}$ correlates the spin qubits. The resulting highly correlated states decay during t_1. The Hamiltonian $\mathcal{H}_{\rm conv}$ converts the remaining order into measurable magnetization, which is then detected as the amplitude of the free induction decay (FID).

in our system). We use proton spins $\left(I=\frac{1}{2}\right)$, which are initially in thermal equilibrium at room temperature and therefore uncorrelated. Under the influence of a suitable Hamiltonian, which consists of couplings between pairs of spins, this uncorrelated state is transformed into a state that involves correlations within clusters of spins. In Fig. 1, which shows the principle of the experiment, the Hamiltonian that generates the correlations is labeled $\mathcal{H}_{\rm corr}$. The size of the spin clusters grows with the time τ for which the correlating Hamiltonian is applied.

After creating these model quantum registers, we let them evolve freely for a time t_1. During this time, the nuclear spins that constitute the quantum register are not isolated from their environment, but couple to other spins by magnetic dipole-dipole interactions. These couplings are the main source of the decoherence processes that increase the entropy of the system. To monitor this decoherence process, we have to measure the remaining order in the quantum register.

A tomographic analysis of this state is not feasible, since the required number of individual measurements increases exponentially with the number of qubits [26]. Instead, we measure the fidelity of the memory channel,

$$F_m \propto \mathrm{Tr}\{\rho(\tau)\rho(\tau+t_1)\}.$$

This can be achieved by transferring the amplitude of the state to an observable quantity by reversing the evolution generated by the pumping Hamiltonian $\mathcal{H}_{\rm corr}$. This process is the inverse of the pumping process driven by $\mathcal{H}_{\rm corr}$ and must therefore be generated by the Hamiltonian $\mathcal{H}_{\rm conv}=-\mathcal{H}_{\rm corr}$, acting for the same duration τ. After this conversion step, the information about the decay is stored as longitudinal magnetization and can be measured as the free induction decay (FID) after applying a detection pulse.

B. Hilbert space of N spins 1/2

We consider a system of N spins $I=1/2$ interacting through magnetic dipole-dipole couplings. Using the rotating frame approximation [27] in a strong magnetic field, this system is described by the Hamiltonian

$$\mathcal{H}^{dd}=\sum_{i,j}\frac{d^{ij}}{2}\left\{2I_z^iI_z^j-\frac{I_+^iI_-^j+I_-^iI_+^j}{2}\right\}, \tag{1}$$

where d^{ij} are the coupling constants, I_z^i are the z components of the spin operators, and $I_\pm^i$ are the corresponding raising and lowering operators. The 2^N stationary states of the Hamiltonian can be classified according to the total magnetic quantum number

$$m_t := \sum_{i=1}^{N} m^i \tag{2}$$

of the total spin operator

$$I_z=\sum_i I_z^i,$$

where m^i is the eigenvalue of I_z^i.

In strongly dipolar coupled spin systems, the eigenfunctions $|r\rangle$ of the Hamiltonian $\mathcal{H}^{dd}$,

$$\mathcal{H}^{dd}|r\rangle=\hbar\omega^r|r\rangle, \tag{3}$$

are linear combinations of direct product states with identical m_t, i.e., they are eigenstates of the total spin operator I_z:

$$I_z|r\rangle=m_t^r|r\rangle.$$

The different coherences (equal to off-diagonal elements of the density operator ρ) can therefore be labeled by the difference of the total magnetic quantum numbers. An element ρ_{rs} is called an M quantum coherence if it connects two states $|r\rangle$ and $|s\rangle$ for which

$$M := m_t^r-m_t^s. \tag{4}$$

$M=0$ represents zero-quantum coherences and populations (diagonal elements). Only the single spin, single quantum coherences with $M=\pm1$ are directly observable by magnetic resonance. Therefore, we have to use an indirect detection method to measure the multispin correlations.

C. Creation of the quantum register

The system is initially in thermal equilibrium in a strong magnetic field $\vec{B}_0=B_0\vec{e}_z$. In the high-temperature approximation [27], its density operator is therefore

$$\rho_{\rm eq}=\frac{1}{2^N}\left(\mathbf{1}+\frac{\hbar\gamma B_0}{kT}\sum_i I_z^i\right), \tag{5}$$

where γ is the gyromagnetic ratio of the spins and T is the temperature. The individual qubits are therefore independent of each other.

To create the correlated states, we need a Hamiltonian that does not commute with the equilibrium density operator of Eq. (5) and introduces correlations. A suitable Hamiltonian consists of two-spin interactions, e.g.,

$$\mathcal{H}^{\pm2}=-\sum_{i,j}\frac{d_{ij}}{4}[I_+^iI_+^j+I_-^iI_-^j]. \tag{6}$$

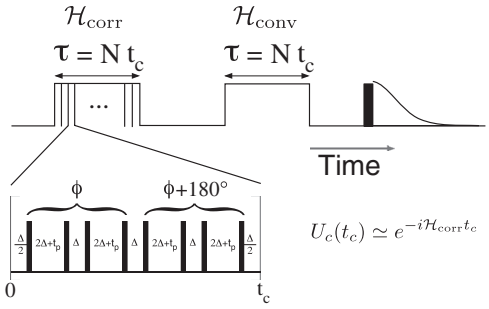

FIG. 2. Pulse sequence for creating the average Hamiltonian $\mathcal{H}_{\rm corr}$. The thick black lines represent $\pi/2$ pulses. The pumping and conversion periods each consist of N repetitions of the basic pulse sequence. For the correlating Hamiltonian $\mathcal{H}_{\rm corr}$ we set $\phi=0°$, and for the reconversion step $\phi=90°$.

For our purpose, it is convenient to use an expansion of the density operator in terms of irreducible tensor operators $\mathbf{A}_{LMK}$

$$\rho(\tau) = e^{-i\mathcal{H}^{\pm 2}\tau}\rho_{\rm eq}e^{i\mathcal{H}^{\pm 2}\tau} = \sum_{LMK} a_{LMK}(\tau)\mathbf{A}_{LMK}, \tag{7}$$

where L, M are the rank and order of the tensor operators and K refers to the number of correlated spins of the specific operator. Additional quantum numbers, which are needed for complete labeling, are omitted for clarity.

The correlating Hamiltonian $\mathcal{H}_{\rm corr}=\mathcal{H}^{\pm 2}$ as well as the reconverting Hamiltonian $\mathcal{H}_{\rm conv}=-\mathcal{H}^{\pm 2}$ are both created as effective average Hamiltonians of a multiple pulse sequence. Figure 2 shows the specific pulse sequence that we used in our experiments. It consists of $\pi/2$ rotations of the spins separated by periods of free precession under the dipolar Hamiltonian of Eq. (1) [28,29]. To an excellent approximation, it generates an overall evolution

$$U_c(t_c) \simeq e^{-i\mathcal{H}_{\rm corr}t_c}. \tag{8}$$

For the reconversion process of the spin clusters back to observable magnetization we apply the same pulse sequence with an overall phase shift of $\phi=90°$ compared to the preparation of the correlated states. This phase shift leads to the desired Hamiltonian:

$$e^{-i(\pi/2)I_z}\mathcal{H}^{\pm 2}e^{i(\pi/2)I_z} = -\mathcal{H}^{\pm 2}. \tag{9}$$

Because of the specific form of the correlating Hamiltonian (6), where raising and lowering operators are paired, we excite only even order coherences if we start our experiments from thermal equilibrium (5).

III. QUANTUM REGISTER SIZE

A. Cluster size vs coherence order

Our quantum registers are clusters of correlated nuclear spins. To determine the register size, we have to measure the number of spins that are correlated by the initial pumping process. A solution for this problem was developed by Baum *et al.* [29]. The basic idea is that in a system of K spins $\frac{1}{2}$, the density operator has

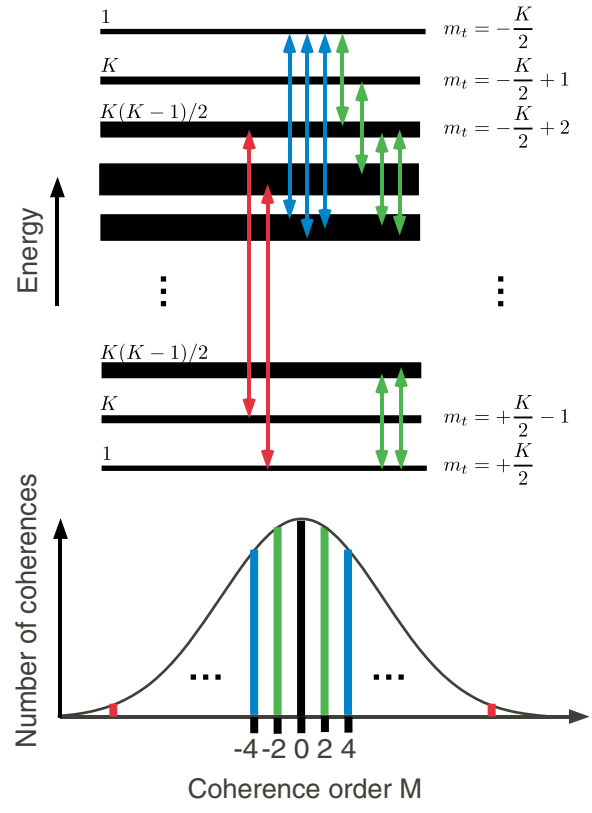

FIG. 3. (Color online) Top: Energy level diagram of a K spin-1/2 system. Each bar represents energy levels with the same total magnetic quantum number m_t. The number of energy levels with a given quantum number m_t is written above the corresponding bar. The arrows connecting different states represent some of the coherences of order $M=m_t^r-m_t^s$. Bottom: Number of coherences with the corresponding order M.

$$\frac{(2K)!}{(K+M)!(K-M)!} \tag{10}$$

M quantum elements. In the statistical model of Baum *et al.*, one assumes that all allowed coherences have comparable amplitudes.

In the upper part of Fig. 3, some of the possible coherences are shown as arrows connecting the involved states in an energy level diagram of K spins 1/2. Each horizontal bar in this figure represents a manifold of energy levels with the same total magnetic quantum number m_t. The number of states

$$\frac{K!}{(K/2-m_t)!(K/2+m_t)!} \tag{11}$$

in such a manifold with the quantum number m_t is written on top of some of the bars.

The basic assumption of the statistical model of Baum *et al.* is that all coherences not forbidden by symmetry are excited with equal probability during the pumping process. In the measured signal, the amplitudes of the coherence order M are therefore equal to the number of M quantum elements of the density operator (10). The lower part of Fig. 3 shows the resulting distribution.

For large K, we may approximate the binomial distribution by a Gaussian $s_M \propto e^{-M^2/K}$. The width of this distribution (full width at half maximum) is $\sigma = 2\sqrt{(\ln 2)K}$. Fitting the signal amplitude s_M as a function of the coherence order M to a Gaussian, we obtain the effective cluster size from the width σ of the distribution.

B. Separating coherence orders

To measure the cluster size, we therefore have to distinguish the different coherence orders of the density operator,

$$\rho = \sum_M \rho_M. \tag{12}$$

The different orders can be distinguished by rotating the state around the z axis,

$$\rho(\Delta\phi) = e^{i\Delta\phi I_z}\rho e^{-i\Delta\phi I_z} = \sum_M e^{iM\Delta\phi}\rho_M. \tag{13}$$

In terms of the irreducible tensor operators $\mathbf{A}_{LMK}$, this becomes

$$\rho(\Delta\phi) = \sum_M e^{iM\Delta\phi}\sum_{LK} a_{LMK}\mathbf{A}_{LMK}. \tag{14}$$

C. Reconversion and measurement

To measure the amount of multiple spin order in the system, we have to convert its amplitude into single spin order, as discussed in Sec. II A. This is achieved by an evolution of the spins for a time τ governed by the conversion Hamiltonian $-\mathcal{H}^{\pm 2}$:

$$\rho(\tau+\tau,\Delta\phi) = e^{-i(-\mathcal{H}^{\pm 2})\tau}\rho(\tau,\Delta\phi)e^{i(-\mathcal{H}^{\pm 2})\tau}. \tag{15}$$

By using the cyclic invariance of the trace operation and $e^{-i\mathcal{H}^{\pm 2}\tau}I_z e^{+i\mathcal{H}^{\pm 2}\tau} = \rho(\tau)$, the longitudinal magnetization after the conversion becomes

$$S(\tau+\tau,\Delta\phi) = \mathrm{Tr}[I_z\rho(\tau+\tau,\Delta\phi)] \tag{16}$$

$$= \mathrm{Tr}[\rho(\tau)\rho(\tau,\Delta\phi)]. \tag{17}$$

Using the irreducible tensor operator base, this is

$$S(\tau+\tau,\Delta\phi) = \sum_M e^{iM\Delta\phi}\sum_{LK}|a_{LMK}(\tau)|^2. \tag{18}$$

Repeating this measurement for fixed τ and a sequence of values $\Delta\phi$, we get the distribution of the coherence amplitudes as a function of M after a Fourier transform of Eq. (18) with respect to $\Delta\phi$. This distribution

$$s_M \sim \sum_{LK}|a_{LMK}(\tau)|^2 \tag{19}$$

is called a multiple quantum spectrum.

D. Experimental details

Experiments were performed at room temperature on a home-built solid-state NMR spectrometer operating at a ^1H frequency of 300 MHz. The proton spins of a powdered adamantane sample served as the spin system.

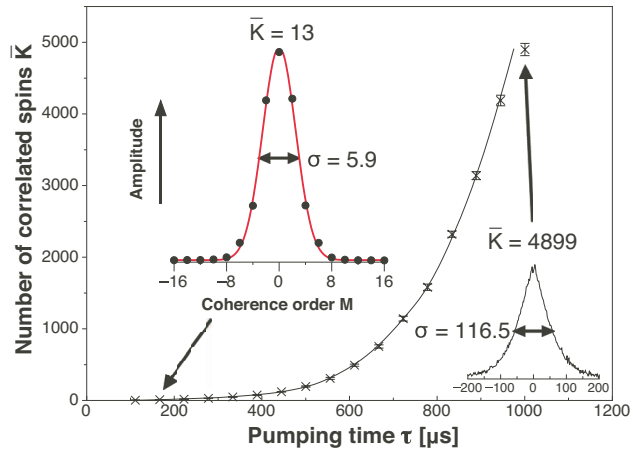

FIG. 4. (Color online) Size $\bar{K}$ of the model quantum register as a function of the excitation time τ. The points represent measured values whereas the solid line is a guide to the eye. The large inset shows the distribution of the coherence amplitudes for a pumping time of $\tau = 167$ μs together with the result of the Gaussian fit to determine the cluster size $\bar{K}$. The small inset shows the multiple quantum spectrum at the longest pumping time of $\tau = 1$ ms.

Because we are using multiple pulse solid state NMR techniques, we set up the spectrometer with suitable tune-up sequences [30–32] before starting the experiments. For the tune-up experiments we used a small spherical water sample where we checked with a network analyzer that the influence of this sample on the probe circuit is the same as that of the adamantane sample used afterwards for the decoherence measurements. Additional to the stroboscopic detection during the tune-up sequences, we observed the phase transients through the reflected power and with a small detection coil located near the sample coil [33].

The longitudinal magnetization I_z was measured by applying a $\pi/2$ pulse and recording the amplitude of the free induction decay (FID).

The size of the qubit register can be adjusted through the preparation time τ. It consists of repetitions of the basic multiple pulse cycle (Fig. 2). We used a $\pi/2$ pulselength of $t_p = 2.448$ μs, and the cycle time was $t_c = 55.584$ μs.

To separate the signal into components with different coherence orders M, we changed the phases of the pumping pulse sequence relative to the fixed phases of the conversion pulse sequence from 0 to 2π in 2^p steps of $\Delta\phi = 2\pi/2^p$, with integer p. The measured signals were then Fourier transformed with respect to ϕ to yield the multiple quantum spectrum. The largest coherence order that can be detected is then $M_{\max} = \pi/\Delta\phi$.

E. Results

We determined the quantum register size $\bar{K}$ as described before for each pumping time τ. Figure 4 summarizes the results: The number of correlated spins $\bar{K}$ increases rapidly with the duration of the excitation time τ. For the longest

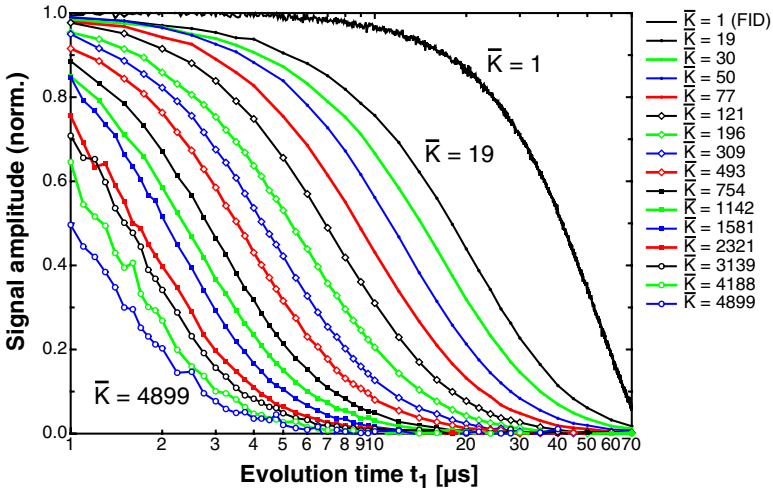

FIG. 5. (Color online) Semilogarithmic plot of the decay of highly correlated spin states. The different data sets connected by lines correspond to different cluster sizes, as listed in the legend. $\bar{K}$ is an average cluster size that we determined in Sec. III E. All curves have been normalized to their values at $t_1=0$. The uppermost curve is the free induction decay (FID) for uncorrelated spin qubits.

pumping time of $\tau=1$ ms, we obtained an effective quantum register size of $\bar{K}=4899$. The corresponding distribution of coherence orders can be seen in the small inset of Fig. 4. The large inset shows the distribution for a much shorter excitation time and the accompanying Gaussian fit. For the correlating Hamiltonian that we used in our experiments, only even-order coherences are excited.

In the next sections, where we discuss the scaling of the decoherence rates, we use the number of correlated spins obtained in this way as the system size.

IV. DECAY UNDER FREE EVOLUTION

A. Evolution and measurement

Decoherence is induced by the coupling of the quantum register to its environment. In our system, the main coupling is the magnetic dipole-dipole interaction between the spins (1). The environment consists of all the roughly 10^{20} spins of the sample.

The density operator after the excitation pulse sequence is Eq. (7)

$$\rho(\tau) = \sum_{LMK} a_{LMK}(\tau)\mathbf{A}_{LMK}.$$

We write the subsequent decay of the coherence during the free evolution of duration t_1 as

$$\rho(\tau + t_1) = \sum_{LMK} f_{LMK}(t_1)a_{LMK}(\tau)\mathbf{A}_{LMK} + \rho', \qquad (20)$$

where f_{LMK} is the correlation function that we want to measure and ρ' are density operator terms that are not observed.

After the conversion step, the density operator is

$$\rho(\tau + t_1 + \tau) = e^{-i(-\mathcal{H}^{\pm 2})\tau}\rho(\tau + t_1)e^{i(-\mathcal{H}^{\pm 2})\tau}, \qquad (21)$$

and the measured signal amplitude S after the detection pulse is therefore

$$S(\tau + t_1 + \tau) = \sum_{LMK} |a_{LMK}(\tau)|^2 f_{LMK}(t_1). \qquad (22)$$

B. Results

The decay of the signal amplitude during the evolution can be seen in Fig. 5 for different cluster sizes $\bar{K}$, which we determined as described before. In addition, the decay of the free induction (FID), i.e., of the uncorrelated spins, is plotted as a reference. The data sets show clearly that the highly correlated states are more fragile than the uncorrelated spins. The shape of the decay curves could be fitted reasonably well to a Gaussian.

For a quantitative dependence of the decoherence rate on the size of the system, we determined rate constants as the inverse of the $1/e$-decay time. In Fig. 6, these decoherence rates are plotted against the system size in a double-logarithmic and a linear plot (inset). The measurements and the fits confirm the approximate square-root scaling that we found recently [13], but now for a much wider range of cluster sizes (up to 4899 correlated spins).

So far we only considered the decay of the total order in the system. More detailed measurements can differentiate between different components of the density operator, which

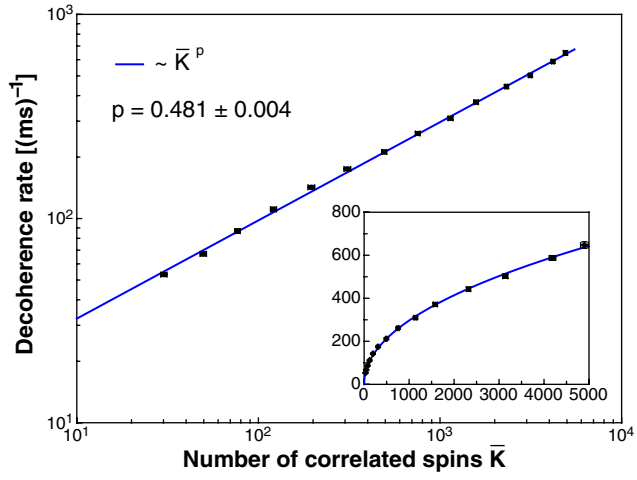

FIG. 6. (Color online) Increase of the decoherence rate for increasing quantum register sizes up to $K=4899$. The points are experimental data. The inset shows the same data with a linear scale. We fit the data to the power function $f(K)=K^p$ (blue line).

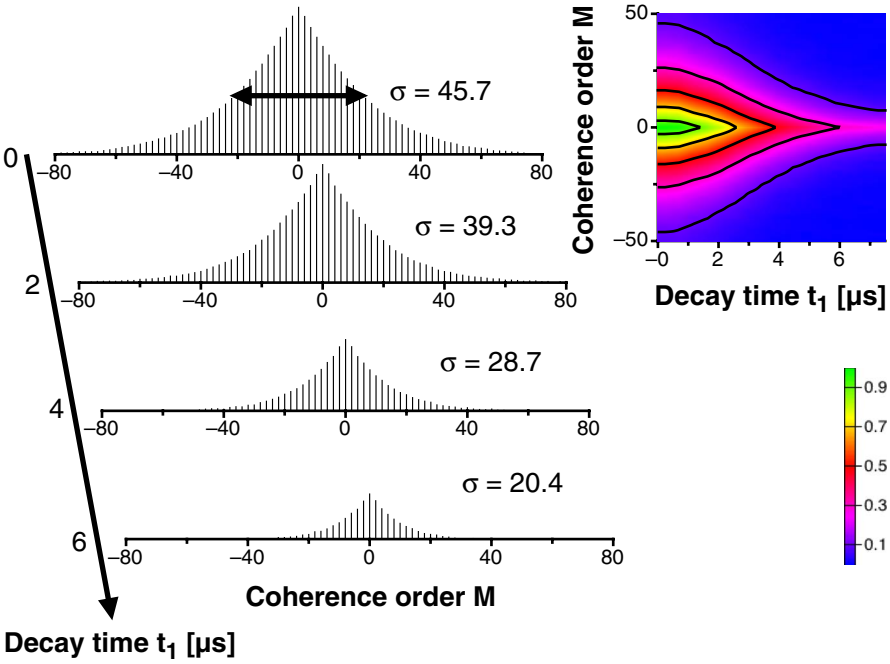

FIG. 7. (Color online) A few multiple quantum spectra for different decay times t_1. In this example, the pumping time was $\tau = 667\ \mu s$ and the average cluster size is $\bar{K}=754$. Furthermore, the measured multiple quantum spectrum amplitudes are shown as contour plots for 16 values of t_1. The bars in the corresponding color scale indicate the values of the contour lines in this plot.

decay at different rates. The simplest differentiation is an independent measurement for different coherence orders M. This can be achieved by repeating the measurement of the multiple quantum spectrum, where the orders M are separated, for different values t_1. If we include the phase shifts $\Delta\phi$ in Eq. (22), we get

$$S(\tau + t_1 + \tau, \Delta\phi) = \sum_M e^{iM\Delta\phi} \sum_{LK} |a_{LMK}(\tau)|^2 f_{LMK}(t_1). \tag{23}$$

The multiple quantum spectrum for an evolution time t_1 now contains the decayed amplitudes

$$s_M(\tau; t_1) \sim \sum_{LK} |a_{LMK}(\tau)|^2 f_{LMK}(t_1), \tag{24}$$

and we can trace the decay of the individual coherence orders as a function of t_1.

The multiple quantum spectra that we obtained for different evolution times t_1 are plotted for $\bar{K}=754$ spins in Fig. 7. Comparison of the spectra shows that at later times, the distribution is narrower, indicating a faster decay of higher order coherences. The color-coded contour plot shows additional data (a total of 16 different t_1 values) for the same quantum register size, again as a function of decay time (horizontal axis) and multiple quantum order (vertical axis).

V. DECOUPLING OF THE QUANTUM REGISTERS FROM THE ENVIRONMENT

To achieve fault-tolerant quantum computation, it is possible to use error-avoiding and error-correcting codes. In addition, minimization of decoherence will be necessary by avoiding and reducing unwanted couplings to the environment, e.g., by "quantum bang-bang control" [16].

In our system, the main coupling between the quantum registers and the environment is the dipole-dipole interaction $\mathcal{H}^{dd}$ (1). Since the interaction strength depends on the orientation of the spins as an irreducible second rank tensor [27], it can be averaged to zero by performing an isotropic average. This procedure is used in so-called homonuclear decoupling experiments [21,34], where sequences of radio-frequency pulses rotate the spins in such a way that the spin-spin coupling vanishes in the average.

These experiments have been very successful for obtaining high-resolution spectra of homonuclear spin systems. For quantum information processing, their performance is more important for large quantum registers. To measure this effect, we used the same system as described above, but replaced the free precession period t_1 with a period of homonuclear decoupling, designed to minimize the decoherence rate.

We tested several decoupling sequences for their performance in slowing down the decay and found similar behavior. In the results presented here, we used the MREV-16 decoupling sequence [23] which is a variation of the standard homonuclear multiple pulse sequence MREV-8 [35,36].

The MREV-16 sequence was corrected for the finite pulse width t_p and the duration of the basic pulse cycle was $t_c(\text{decoupling}) = 111.072\ \mu s$. To follow the decay of the coherence, we repeated the experiment with different evolution periods t_1, using up to 32 MREV-16 cycles. The longest evolution time was thus approximately 3.6 ms.

In the semilogarithmic plot of Fig. 8 we compare the decay of the quantum registers for the case of free evolution and homonuclear decoupling for six different cluster sizes $\bar{K}$. The decay curves are normalized to the maximum amplitude at $t_1=0$.

The large distance of more than an order of magnitude between the two groups of curves clearly shows that all quantum registers survive much longer when we reduce the coupling of the quantum registers to their environment, i.e.,

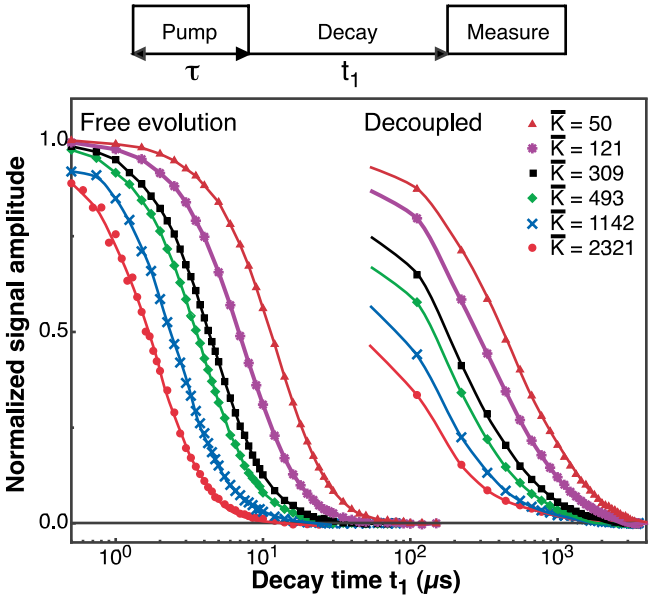

FIG. 8. (Color online) Effect of decoupling for six different cluster sizes. The six left curves are for free evolution (see Fig. 5) and those on the right-hand side for decoupling of the quantum registers. The normalization of the signal amplitude is in both cases relative to the value at $t_1=0$.

the surrounding spins. While the form of the decay remains qualitatively similar to the case of free evolution, the decoupled decays show some differences in the long-time part of the decay curves: An exponential yields the better fit, while the free decay is better described by a Gaussian. Since the shortest decay time is determined by the cycle time t_c(decoupling), which is ≈ 111 μs in our case, it is difficult to observe the beginning of the decay, which might be useful for measuring the onset of the decay.

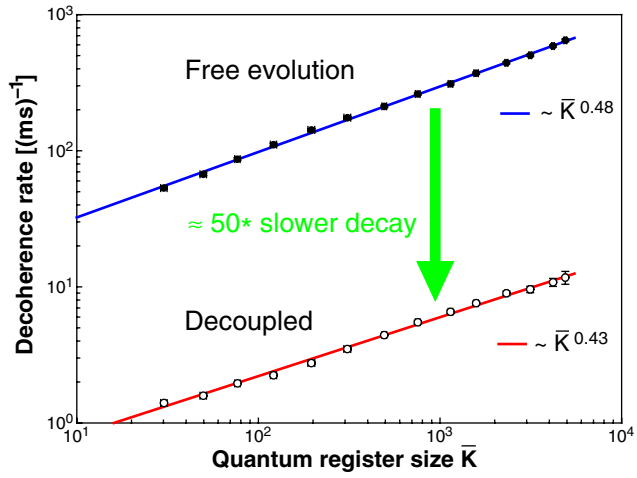

FIG. 9. (Color online) Average decoherence rates for the two cases of free evolution and homonuclear decoupling of the dipolar coupled spins during t_1.

We determined the decoherence rates for various cluster sizes as in the free evolution measurements to obtain the scaling under homonuclear decoupling. This is compared in Fig. 9 with the case of free evolution. The reduction of the decoherence rates appears to work even better for larger clusters: For the decoupled case, our fit to a power law $\propto \bar{K}^p$ yields an exponent $p=0.43$, compared to $p=0.48$ for the free evolution decay.

Like in the case of free evolution, we can also measure the decay of different coherence orders M independently by taking multiple quantum spectra for different decay times t_1 (compare to Fig. 7). Figure 10 shows the resulting decay curves for different cluster sizes and different coherence orders. The left-hand column corresponds to the free evolution and the right-hand side to the decoupled case. Note the dif-

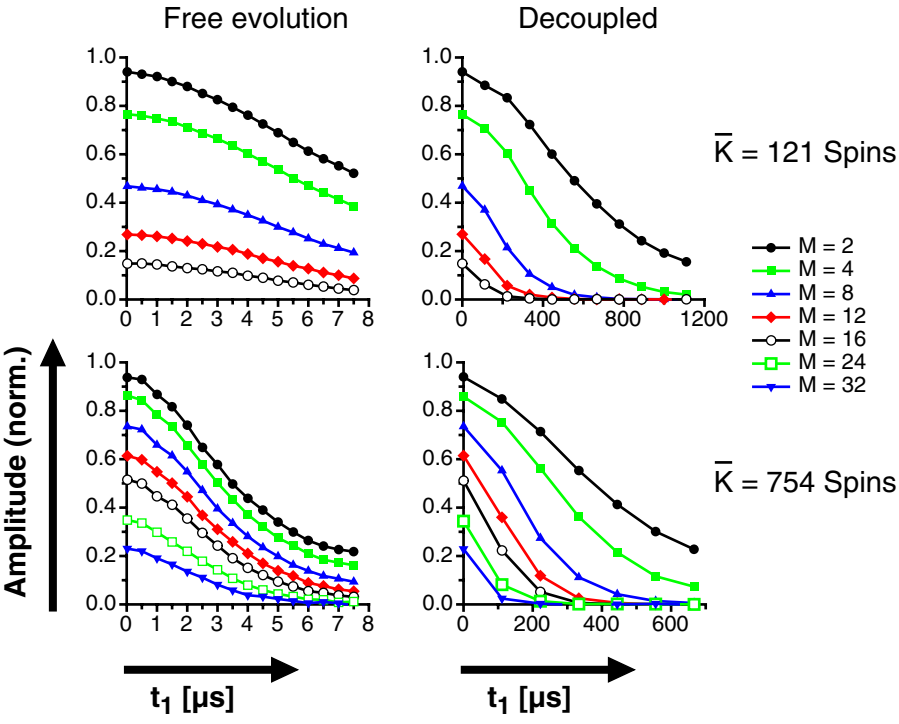

FIG. 10. (Color online) Decay of individual coherence orders M. The two upper data sets are from a small quantum register ($\bar{K}=121$); the two lower sets are from a larger one ($\bar{K}=754$). In all four plots the data points are normalized to the maximum amplitude at $t_1=0$ and $M=0$. The decay of all coherence orders is slowed down under MREV-16 decoupling (right-hand side) compared to the free evolution (left-hand side), as visible from the different time scales on the left and right figures.

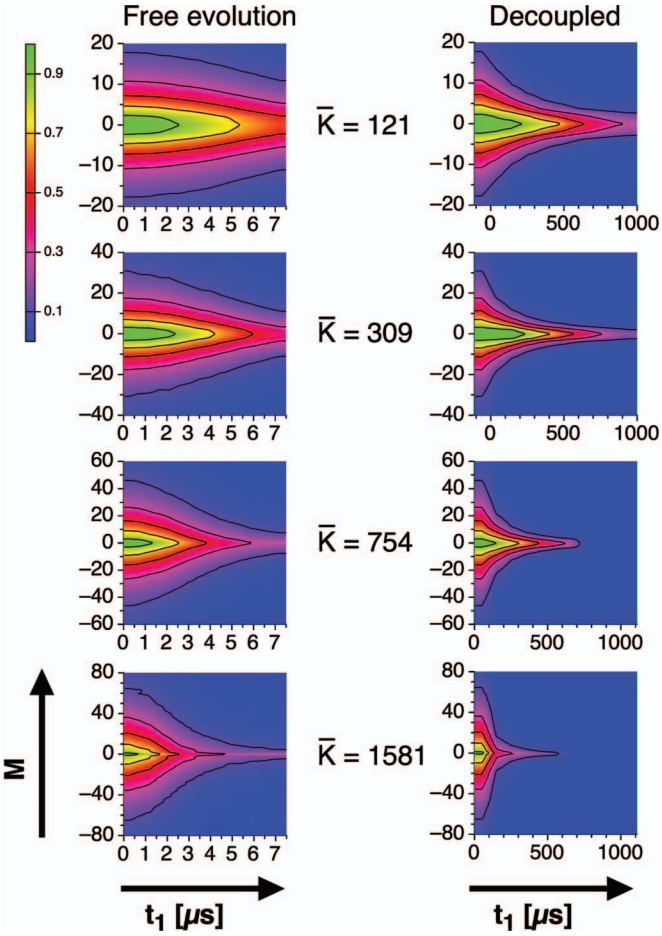

FIG. 11. (Color online) Comparison of the decay of the coherence orders M with t_1 for four different quantum register sizes $\bar{K}$. All the multiple quantum spectrum amplitudes shown as contour plots are normalized to their $t_1=0$, $M=0$ signal intensity.

ferent time scales of the two columns. Like in the integral measurements of Fig. 8, these data show a significant extension of the coherence lifetimes by almost two orders of magnitude.

In both cases (free evolution and decoupling), higher order coherences decay more rapidly than lower order coherences. This behavior can be explained by the fact that each K-spin cluster contributes only to signal components of order $M \leqslant K$. Higher order coherences contain therefore bigger contributions from large clusters, which decay faster (see Fig. 8).

Figure 11 shows the decay of all excited coherence orders for different cluster sizes. The color-coded (online version) contour plots represent the order in the system as a function of the decay time t_1 (horizontal axis) and coherence order (vertical axis). For each system size, we compare the decay under free evolution with the decoupled case. The data sets were obtained by measuring the multiple quantum amplitudes, as discussed in Sec. IV B, for different decay times t_1. Note the different time scale of the plots in the right-hand column.

VI. DISCUSSION AND CONCLUSION

In conclusion, we measured the scaling behavior of the decoherence rates in model quantum registers consisting of several 1000 nuclear spins. The model quantum registers are clusters of correlated spins, and all the roughly 10^{20} spins of the sample constitute the environment. The differentiation between system and environment is made by the detection process, which measures the autocorrelation function of the spin clusters.

In addition to the measurements of the average decoherence rates (Fig. 6), we measured the decay of individual coherence orders M. The results show that the decay is faster for higher orders. A more detailed characterization of the decay for individual spin operators $\mathbf{A}_{LMK}$ would be possible by rotating the system around two orthogonal axes [37–39] or by spherical tensor analysis [40]. Such measurements might give more insight into the spread of the individual coherences and their decoherence rates. However, for the operation of a quantum computer, the most important parameter is the average decoherence rate: During a quantum computation, the information does not remain in any specific area of Hilbert space, where it might decay with a specific decoherence rate, but it is repeatedly rearranged over the full Hilbert space of the quantum register. The information will therefore decay with an average decoherence rate [41].

We also could show experimentally that the decoherence time of highly correlated spin states can be extended by more than an order of magnitude by decoupling the quantum register from its environment. The efficiency of this decoupling technique does not depend significantly on the size of the system, thus suggesting that this approach may remain useful for arbitrarily large quantum information processors. In our system, the decoherence rate could be reduced by a factor of 50. At this stage, it remains unclear what causes the remaining decoherence. Imperfect decoupling contributes to this, but is difficult to quantify exactly. This issue has been discussed for different pulse sequences (see, e.g., Ref. [42]). In this case, the decoherence times were measured for uncorrelated spins and found to be an order of magnitude shorter than the relaxation times due to irreversible processes (e.g., spin-lattice relaxation).

In the case of free evolution as well as when we applied the decoupling sequence, the decoherence rate increases with the size of the quantum register. This increase is significantly less than linear, as can be seen in Fig. 9. This suggests that the perturbations that act on different qubits are correlated, because if they were completely uncorrelated, a linear increase of the decoherence rate with the qubit register size would be expected [2,43].

An initial theoretical analysis of these findings considers correlations of the multiqubit decoherence [44]. A certain degree of correlation should be present in all physical systems proposed for quantum information processing. The scaling behavior of the overall decoherence can be improved by encoding the qubits in suitable areas of Hilbert space [41].

The shape of the free evolution decay (see Fig. 5) indicates that the interaction with the environment is a non-Markovian process. If we apply decoupling, the decay resembles more an exponential curve (see Fig. 8). This may

indicate that, in this case, the interaction can be modeled as a Markovian process. We are currently testing the details of this process in a system where the system and environment can be addressed independently [45].

If our results of the relatively benign scaling of the decoherence rates and the efficiency of decoupling sequences can be verified in other systems, it raises the prospects for implementing large-scale quantum computers in solid-state systems.

ACKNOWLEDGMENTS

The authors thank Marko Lovrić for technical support and the Deutsche Forschungsgemeinschaft for financial support through the Graduiertenkolleg 726.

[1] P. W. Shor, in *Proceedings of the 35th Annual Symposium on the Foundations of Computer Science*, edited by S. Goldwasser (IEEE Computer Society Press, Los Alamitos, CA, 1994), p. 124.
[2] W. G. Unruh, Phys. Rev. A **51**, 992 (1995).
[3] J. E. Mooij, T. P. Orlando, L. Levitov, L. Tian, C. H. van der Waal, and S. Lloyd, Science **285**, 1036 (1999).
[4] D. Loss and D. P. DiVincenzo, Phys. Rev. A **57**, 120 (1998).
[5] J. I. Cirac and P. Zoller, Phys. Rev. Lett. **74**, 4091 (1995).
[6] B. Kane, Nature (London) **393**, 133 (1998).
[7] D. G. Cory *et al.*, Fortschr. Phys. **48**, 875 (2000).
[8] R. Vrijen, E. Yablonovitch, K. Wang, H. W. Jiang, A. Balandin, V. Roychowdhury, T. Mor, and D. DiVincenzo, Phys. Rev. A **62**, 012306 (2000).
[9] W. Harneit, C. Meyer, A. Weidinger, D. Suter, and J. Twamley, Phys. Status Solidi B **233**, 453 (2002).
[10] D. Suter and K. Lim, Phys. Rev. A **65**, 052309 (2002).
[11] T. D. Ladd, J. R. Goldman, F. Yamaguchi, Y. Yamamoto, E. Abe, and K. M. Itoh, Phys. Rev. Lett. **89**, 017901 (2002).
[12] M. Mehring and J. Mende, Phys. Rev. A **73**, 052303 (2006).
[13] H. G. Krojanski and D. Suter, Phys. Rev. Lett. **93**, 090501 (2004).
[14] B. J. Preskill, Proc. R. Soc. London, Ser. A **454**, 385 (1998).
[15] M. A. Nielsen and I. L. Chuang, *Quantum Computation and Quantum Information* (Cambridge University Press, Cambridge, UK, 2000).
[16] L. Viola and S. Lloyd, Phys. Rev. A **58**, 2733 (1998).
[17] P. Facchi, S. Tasaki, S. Pascazio, H. Nakazato, A. Tokuse, and D. A. Lidar, Phys. Rev. A **71**, 022302 (2005).
[18] E. L. Hahn, Phys. Rev. **80**, 580 (1950).
[19] H. Y. Carr and E. M. Purcell, Phys. Rev. **93**, 749 (1954).
[20] S. Meiboom and D. Gill, Rev. Sci. Instrum. **29**, 688 (1958).
[21] J. S. Waugh, L. M. Huber, and U. Haeberlen, Phys. Rev. Lett. **20**, 180 (1968).
[22] E. Fraval, M. J. Sellars, and J. J. Longdell, Phys. Rev. Lett. **95**, 030506 (2005).
[23] T. D. Ladd, D. Maryenko, Y. Yamamoto, E. Abe, and K. M. Itoh, Phys. Rev. B **71**, 014401 (2005).
[24] J. Baugh, O. Moussa, C. A. Ryan, R. Laflamme, C. Ramanathan, T. F. Havel, and D. G. Cory, Phys. Rev. A **73**, 022305 (2006).
[25] H. G. Krojanski and D. Suter, Phys. Rev. Lett. **97**, 150503 (2006).
[26] I. L. Chuang, N. Gershenfeld, M. Kubinec, and D. W. Leung, Proc. R. Soc. London, Ser. A **454**, 447 (1998).
[27] A. Abragam, *The Principles of Nuclear Magnetism* (Oxford University Press, Oxford, 1961).
[28] W. S. Warren, S. Sinton, D. P. Weitekamp, and A. Pines, Phys. Rev. Lett. **43**, 1791 (1979).
[29] J. Baum, M. Munowitz, A. Garroway, and A. Pines, J. Chem. Phys. **83**, 2015 (1985).
[30] M. Mehring and J. S. Waugh, Rev. Sci. Instrum. **43**, 649 (1972).
[31] U. Haubenreisser and B. Schnabel, J. Magn. Reson. (1969-1992) **35**, 175 (1979).
[32] D. P. Burum, M. Linder, and R. R. Ernst, J. Magn. Reson. (1969-1992) **43**, 463 (1981).
[33] J. D. Ellet, Jr., M. G. Gibby, U. Haeberlen, L. M. Huber, M. Mehring, A. Pines, and J. S. Waugh, Adv. Magn. Reson. **5**, 117 (1971).
[34] U. Haeberlen and J. S. Waugh, Phys. Rev. **175**, 453 (1968).
[35] P. Mansfield, M. J. Orchard, D. C. Stalker, and K. H. B. Richards, Phys. Rev. B **7**, 90 (1973).
[36] W.-K. Rhim, D. D. Elleman, and R. W. Vaughan, J. Chem. Phys. **59**, 3740 (1973).
[37] D. Suter and J. Pearson, Chem. Phys. Lett. **144**, 328 (1988).
[38] C. Ramanathan, H. Cho, P. Cappellaro, G. S. Boutis, and D. G. Cory, Chem. Phys. Lett. **369**, 311 (2003).
[39] H. Cho, D. G. Cory, and C. Ramanathan, J. Chem. Phys. **118**, 3686 (2003).
[40] J. D. van Beek, M. Carravetta, G. C. Antonioli, and M. H. Levitt, J. Chem. Phys. **122**, 244510 (2005).
[41] C. S. Maierle and D. Suter, in *Quantum Information Processing*, edited by G. Leuchs and T. Beth (Wiley-VCH, Weinheim, 2003), pp. 121–130.
[42] D. G. Cory, J. B. Miller, and A. N. Garroway, J. Magn. Reson. (1969-1992) **90**, 205 (1990).
[43] G. M. Palma, K.-A. Suominen, and A. K. Ekert, Proc. R. Soc. London, Ser. A **452**, 567 (1996).
[44] A. Fedorov and L. Fedichkin, J. Phys.: Condens. Matter **18**, 3217 (2006).
[45] M. Lovrić, H. G. Krojanski, and D. Suter (unpublished).